Separation Science and Technology
Publication details, including instructions for authors and subscription information:
http://www.informaworld.com/smpp/title~content=t713708471

Biofilm Structure and Extracellular Polymeric Substances in Low and High Dissolved Oxygen Membrane Bioreactors

Hee Yoon Kim[a]; Kyung-Min Yeon[a]; Chung-Hak Lee[a]; Sangho Lee[b]; Tyagarajan Swaminathan[c]
[a] School of Chemical and Biological Engineering, Seoul National University, Seoul, Korea [b] Korea Institute of Construction Technology, Gyeonggi-Do, Korea [c] Department of Chemical Engineering, Indian Institute of Technology, Madras, India

To cite this Article Kim, Hee Yoon , Yeon, Kyung-Min , Lee, Chung-Hak , Lee, Sangho and Swaminathan, Tyagarajan(2006) 'Biofilm Structure and Extracellular Polymeric Substances in Low and High Dissolved Oxygen Membrane Bioreactors', Separation Science and Technology, 41: 7, 1213 — 1230
To link to this Article: DOI: 10.1080/01496390600632354
URL: http://dx.doi.org/10.1080/01496390600632354

Separation Science and Technology, 41: 1213–1230, 2006

ISSN 0149-6395 print/1520-5754 online
DOI: 10.1080/01496390600632354

Biofilm Structure and Extracellular Polymeric Substances in Low and High Dissolved Oxygen Membrane Bioreactors

Hee Yoon Kim, Kyung-Min Yeon, and Chung-Hak Lee
School of Chemical and Biological Engineering, Seoul National University, Seoul, Korea

Sangho Lee
Korea Institute of Construction Technology, Gyeonggi-Do, Korea

Tyagarajan Swaminathan
Department of Chemical Engineering, Indian Institute of Technology, Madras, India

Abstract: This paper discusses the effect of dissolved oxygen (DO) on the biofilm structure in membrane bioreactor (MBR) and their consequence on membrane permeability and EPS. Two MBRs under high DO (6.0 mg/L, HDO) and low DO (<0.1 mg/L, LDO) were operated in parallel under same hydrodynamic conditions. The microbiological aspects in MBR systems were explored through a series of analysis techniques including PCR-DGGE, gel filtration chromatography (GFC), confocal laser scanning microscope (CLSM), and image analysis.

The rate of membrane fouling for the LDO MBR was 5 times faster than that for the HDO MBR. The microbial communities between HDO and LDO MBR were quite different, which is likely to be the reason for different structures and permeabilities of the biofilms. The specific biofilm resistance in HDO MBR was lower to that in LDO MBR. This is attributed to relatively lower porosity and higher amount of EPS for the biofilm in LDO MBR. The distributions of cell and EPS were not uniform in the biofilms in both HDO and LDO MBR. The biofilm in

Received 5 December 2005, Accepted 21 February 2006
Address correspondence to Chung-Hak Lee, School of Chemical and Biological Engineering, Seoul National University, Seoul 151-744, Korea. Tel.: +82-2-880-7075; Fax: +82-2-888-1604. E-mail: leech@snu.ac.kr

LDO MBR contained larger amount of EPS than that in HDO MBR. The ratio of protein to polysaccharide was also higher for biofilm in HDO MBR than in LDO MBR.

Keywords: Membrane bioreactor, biofilm, dissolved oxygen, extracellular polymeric substances, membrane filterability

INTRODUCTION

Membrane bioreactor (MBR) system requires better control of membrane fouling as it demands frequent cleaning and replacement of membranes resulting in increased operating cost (1, 2). Moreover, reliable values of flux decline are necessary for process design (3). Therefore, factors affecting membrane fouling in MBR systems have been widely studied with respect to operating conditions (4, 5) and microbial characteristics (6–8).

Dissolved oxygen (DO) concentration is an important operating parameter controlling biological wastewater treatment process. DO affects the organic removal rate as well as microbial characteristics such flocculation and settling property (9–12). Moreover, switching the oxygen level becomes necessary for a successful biological nutrient removal. It has been reported that low DO condition for the purpose of the nitrogen or phosphorous removal caused the severe permeability loss in membrane bioreactor (11, 13, 14). The reported reasons for the decline of membrane flux at low DO condition are:

1. Increase in the concentrations of soluble components.
2. Increase in specific cake resistance due to smaller microbial floc size.

However, relatively little attention has been paid to the correlation between extracellular polymeric substances (EPS) and membrane fouling in low DO conditions. Moreover, direct characterization of biofilm together with mixed liquor is also required since the physicochemical and microbial characteristics in bulk solution might be different from those in the biofilm.

The objective of this study was to compare membrane permeability and microbial characteristics between two MBR systems under low DO and high DO conditions. The biofilm structure was examined by analyzing the structural parameters using confocal laser scanning microscope (CLSM) combined with image analysis techniques. The microbial communities were identified using 16S-rDNA based molecular biological techniques and the soluble EPS formed under different oxygen levels was characterized using gel filtration chromatography (GFC).

MATERIALS AND METHODS

Reactor Operation

The schematic diagram of MBR is shown in Fig. 1. Two MBR systems with high DO (6.0 mg/L) and low DO (<0.1 mg/L), designated as HDO and LDO MBR, respectively were run in parallel. Air was supplied to HDO MBR, whereas a mixture of air and N_2 to LDO MBR to regulate DO concentration while maintaining the same gas flow rate. This allows providing the same mixing intensity in bioreactors under different dissolved oxygen concentrations. A hollow fiber membrane module was immersed in each reactor. The synthetic wastewater was supplied continuously to the reactor while the membrane permeate was continuously collected by a peristaltic pump under a constant flux ($20\,Lm^{-2}h^{-1}$). The transmembrane pressure (TMP) build-up during the operation, which indicates the extent of membrane fouling was continuously monitored. The operation was stopped to analyze the fouled membrane when TMP reached 30 kPa. Hydraulic retention time (HRT) was set to 12 hrs while solid retention time (SRT) to 20 days by sludge withdrawal. Other detailed operating conditions are shown in Table 1. The COD of synthetic wastewater was 700 mg/L and its composition was shown in Table 2. The membrane was a hydrophilic polyethylene type with a pore size of 0.4 μm (Mitsubishi Rayon, Japan) and an effective area of $0.10\,m^2$.

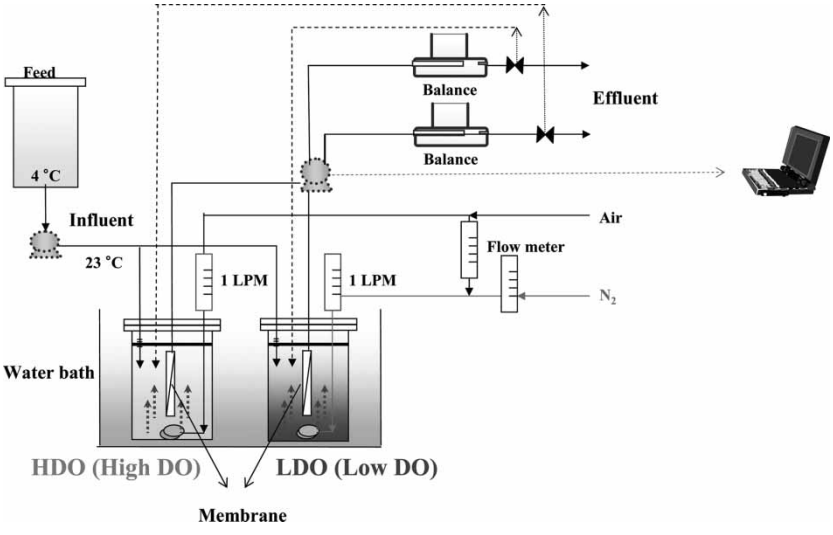

Figure 1. Schematic diagram of the submerged MBR system: HDO and LDO.

Table 1. Operational parameters

	Low DO MBR (LDO)	High DO MBR (HDO)
DO concentration (mg/L)	<0.1	6.0
Aeration rate (L/min)	0.8 (N_2) + 0.2 (Air)	1.0 (Air)
Permeate flux (L/m^2 hr)	20	
Temperature (°C)	23 ± 2	
pH	7 ± 0.8	
Volume (L)	4	
Feed COD (mg/L)	700 ± 23	
Hydraulic retention time (h)	12	
Sludge retention time (d)	20	
MLSS (mg/L)	2000 ~ 3000	7000 ~ 8000

Analysis of Hydraulic Resistances

The resistance-in-series model was applied to evaluate the portion of each resistance of the total resistance in equation (1) according to Choo and Lee (15).

$$J = \frac{\Delta P}{\eta \cdot R_t} = \frac{\Delta P}{\eta(R_m + R_c + R_f)} \tag{1}$$

where J; permeate flux, ΔP; transmembrane pressure, η; viscosity of the permeate, R_t; total resistance, R_m; intrinsic membrane resistance, R_c; cake resistance, R_f; fouling resistance due to any irreversible adsorption/adhesion of molecules.

Table 2. Composition of synthetic wastewater

Composition	Concentration (mg/L)
$C_6H_{12}O_6$	120.00
Bacto peptone	90.00
Yeast extract	12.00
$(NH_4)_2SO_4$	96.00
KH_2PO_4	19.20
$MgSO_4 \cdot 7H_2O$	24.00
$MnSO_4 \cdot 7H_2O$	2.16
$FeCl_3 \cdot 6H_2O$	0.12
$CaCl_2 \cdot 2H_2O$	2.40

Biofilm Analysis

Cross-Sectional Images of Biofilm on Membrane

After the MBR operation was terminated, the hollow fiber membrane module was removed from the reactor. The bundle of hollow fiber membranes (3–10 fibers) with the adhering biofilm on the membrane surface was cut to a length of approximately 10 mm and then fixed in 4% paraformaldehyde solution for 2–8 hrs in a 1.5 mL eppendorf tube at 4°C. The specimen (adhering biofilm + membrane) was then rinsed twice with phosphate-buffered saline. Each rinsed specimen was embedded in OCT compound (Tissue-Tek4583, Miles Inc., USA) overnight to permit the OCT compound to infiltrate the biofilm, and the sample was then frozen at −20°C (16). The frozen specimen was cut into 20 mm-thick slices with a cryotome (HME 504, Germany) at −20°C. Each slice was placed on the gelatin-coated microscopic slide and air dried overnight. The specimen was finally dehydrated by successive 50%, 80%, and 98% ethanol washes (for 3 min each), air dried, and stored at room temperature. The ethanol dehydration procedure substantially reduced the level of OCT compound present (16). A microscope (Eclipse E600, DXM 1200, Nikon) was used to examine the cross-section image of the specimen (biofilm + membrane).

Biofilm Staining and Confocal Laser Scanning Microscopy

The biofilm was stained as described in other studies related to biofilm analysis using CLSM (17, 18). The bacteria, polysaccharide, and protein in the biofilm were stained with SYBR Green I (Molecular Probes, Eugen USA), fluorescently labeled lectins and Hoechst 2495 for multi-staining. Each SYBR Green I, fluorescently labeled lectins and Hoechst 2495 has specificity to nucleic acid, polysaccharide, and protein respectively. The biofilm was incubated for 30 min at room temperature in the dark and was then washed with phosphate buffered saline (PBS) solution. The specifications for each fluorescent probe are summarized in Table 3. Two fluorescently labeled lectins, Concanavaline A and Wheat Germ Agglutinin tetramethyl rhodamine isothiocyanate conjugate (Molecular probes, Eugene, USA), were selected.

Table 3. Fluoroscent probes and their spectral characteristics

Probes	Label	Abs. (nm)	Em. (nm)	Specificity
SYBR Green I	—	488	515/30	Nucleic acid (cell)
Concanavaline A	TRITC	568	600/50	α-Man, α-Glu (polysaccharide)
Wheat Germ Agglutinin	TRITC	568	600/50	(β-GlcNAc)$_2$, NeuNAc (polysaccharide)
Hoechst 2495	—	395	450/80	Protein

After staining, the treated biofilm was immediately observed using a confocal laser scanning microscope system (Radiance 2000, Bio-Rad, UK) comprised of a microscope (Nikon, Japan) and krypton-argon mixed gas laser source. Signals were recorded in the green channel (excitation 488 nm, emission 515/30 nm), red channel (excitation 568 nm, emission 600/50 nm) and blue channel (excitation 395 nm, emission 450/80 nm). For observation, an oil lens with 40 × 1.3 NA lens was used. The Confocal Assistant software supplied by the manufacturer was used to develop the 3-D digitized image, on which the estimation of total cell volume was based. The magnification was ×600. In most cases, optical section with a step size of 1 μm was obtained.

Analysis of CLSM Images

The porosity and coverage of cells and EPS were calculated from the CLSM images to describe biofilm structures under different DO conditions. The software of Image Structure Analyzer-2 (ISA-2) developed by Beyenal (19) was used to estimate the overall porosity and the areal porosity for cell and EPS in each section (20).

Physico-Chemical Analysis

Characteristics of Microbial Floc

Mixed liquor suspended solids (MLSS) was measured using the analytical methods described in the Standard methods (21). The chemical oxygen demand (COD) was measured using the spectrometric method with a reagent kit (HACH, USA). The concentration of DO was measured with a DO meter (WTW, Germany). The specific cake resistance was measured using an unstirred cell unit under a dead-end filtration mode (22). The size distribution of the aggregates in suspension was measured using a laser light-scattering device (Malvern Mastersizer/E, UK). The highest frequency value of the distribution curve was adopted to be the apparent diameter of the aggregates. The fractal dimensions were estimated from the measured intensity of scattered laser light (632.8 nm) obtained from 31 light-sensitive detectors over scattering angles from 0.03 to 6.25° (300-mm lens) (23). For each of the values of the sizes and fractal dimensions, the average value of four raw measurements was taken to be a single data point.

Analysis of EPS: Concentration and Molecular Weight Distribution

In EPS analysis, the bound EPS that are combined with cells to form microbial flocs were differentiated from the soluble EPS that exist in bulk phase as free form (6). Bound EPS was extracted from microbial flocs as well as from biofilm by heating method. Soluble EPS was obtained by filtering the mixed

liquor of the bioreactor with 0.45 μm filter and concentration of typical EPS components such as polysaccharides and proteins were measured. When extracting EPS from the biofilm, the biofilm on the membrane surface was detached in 200 mL of distilled water following the procedure described by Park (24). The concentration of polysaccharide was measured using phenol-sulfuric acid method (25) with glucose as a standard. Protein concentration was measured using modified Lowry method with bovine serum albumin as a standard (26).

The EPS composition was characterized by measuring the molecular weight distribution of EPS using gel filtration chromatography (GFC). A high performance Liquid chromatograph system (HP1100, Hewlett Packard, USA) equipped with Ultrahydrogel 250 column (Waters, USA) was used to carry out GFC. The mobile phase was the $NaNO_3$ (0.1 mM) solution and flow rate was 1 mL/min. Dextrans and polyethylene glycols (PEG) with molecular weights ranging from 4.2×10^2 to 6.7×10^5 Dalton were used as standards. The detection was carried out using both a UV (250 nm) and a refractive index detectors. Prior to the analysis, all samples were filtered with 0.45 μm filter.

Microbiological Analysis

For PCR-DGGE and DNA sequencing, cells harvested from broth or from biofilm attached on membrane surface (24) were processed using an UltraClean™ Soil DNA Isolation Kit (MOBIO, USA). PCR amplification of 16S rDNA was carried out using universal bacteria primers, Duniv336F-GC-clamp and Duniv 529R, and Perfect Premix reagent (TaKaRa, Japan). Thermal cycling was performed with initial denaturation at 94°C for 5 min, followed by 30 cycles of denatuation (at 94°C, 30 sec), annealing (56°C, 30 sec) and extension (72°C, 30 sec) in a thermal cycler (Bio-Rad, USA). The PCR-amplified DNA fragments were separated on the polyacrylamide gels (8%) with a 40 to 60% linear gradient of denaturant. Gels were run for 15 min at 25 V and thereafter for 6 hours at 200 V. After electrophoresis, gels were stained for 30 min with ethidium bromide and scanned with a Gel Documentation System (Gel Doc™ 2000, Bio-Rad, USA). After the sequence of each DGGE band was analyzed, they were compared with sequences in National Center for Biotechnology Information (NCBI) using the basic local alignment search tool (Blast).

RESULTS AND DISCUSSION

Membrane Permeability in HDO and LDO MBR

TMP build-up under constant flux mode has been monitored for HDO and LDO MBR until TMP reached 30 kPa. As shown in Fig. 2, TMP rise in

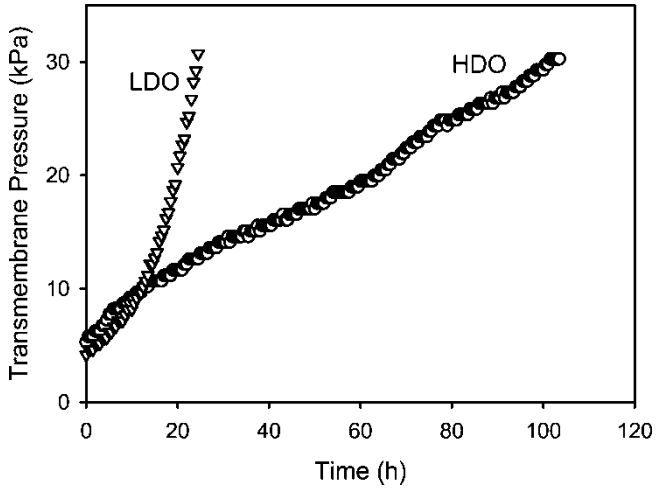

Figure 2. Comparison of transmembrane pressure (TMP) in LDO and HDO MBRs.

LDO MBR was about five times faster than that in the HDO MBR although the MLSS concentration in LDO MBR was only around 1/3 of that in HDO MBR (Table 1). This means that the membrane fouling for LDO MBR was more severe than for HDO MBR. Similar results were also reported in previous studies (14).

In order to identify the main contributor to membrane fouling in each reactor, a hydraulic resistance analysis of the used membrane was conducted after the operation ended at 30 kPa for each MBR. Table 4 shows various resistances calculated with flux data after the operating periods of 105 hr (HDO MBR) and 22 hr (LDO MBR), respectively. The cake resistance (R_c) represented more than 73% of the total resistance in each reactor. This result indicates that cake resistance caused by the formation of a biofilm on the membrane surface was mainly responsible for the filterability loss.

Table 4. Analysis of hydraulic resistances in two MBR systems

	HDO MBR	LDO MBR
Time to reach 30 kPa, (h)	105	22
Resistance ($10^{12}\,m^{-1}$)		
R_m	0.72 (13.3)	0.72 (13.3)
R_c	4.04 (74.8)	3.97 (73.5)
R_f	0.64 (11.9)	0.71 (13.2)
R_t	5.40 (100.0)	5.40 (100.0)

(): the percentage of each resistance of the total one.

Microbial Community in Mixed Liquor and Biofilm

The difference in membrane permeability between HDO and LDO MBR may be attributed to the difference in microbial community. Although the same activated sludge was used for seeding in each reactor, different DO conditions might have changed the microbial community during the acclimation period. PCR-DGGE analysis followed by DNA sequencing was performed to compare the structures of microbial community in two reactors after the MBR operation was terminated. Figure 3 shows the PCR-DGGE patterns in which each band represents a specific microorganism. Bands in samples 1 and 3, from the broth and biofilm in LDO reactor were identical and those in samples 2 and 4, from the broth and biofilm in HDO reactor were identical. This indicates that the microbial communities in HDO and LDO MBRs were different although the microbial communities in broth and biofilm of each reactor were the same. It appears that there is no specific attachment or growth of certain microorganisms on the membrane surface during MBR operation.

To further analyze the microbial species, each band in PCR-DGGE profiles was identified using DNA sequencing methods (Table 5). Six microorganisms were identified in each MBR. The microorganisms in two MBRs were totally different although the same activated sludge was used for seeding. It is evident from Table 5, that difference in DO conditions

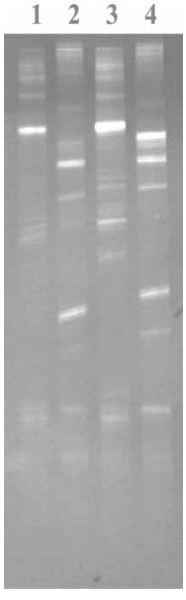

Figure 3. DGGE profile of bacterial communities in HDO and LDO MBRs. 1: LDO bulk solution; 2: HDO bulk solution; 3: LDO biofilm; 4: HDO biofilm.

Table 5. Idenification of microbial communities in HDO and LDO MBRs

Reactor	Species	Similarity (%)
HDO MBR	*Pandoraea sp.*	100
	Bacillus sp.	98.82
	Sphingomonas sp.	94.44
	Citrobacter sp.	100
	Citrobacter freundii	100
	Kluyvera ascorbata	100
LDO MBR	*Azospirillum irakense*	96.55
	Flavobacterium mizutaii	93.02
	Acinetobacter sp.	96.41
	Rhizobium sp.	93.06
	Stenotrophomonas maltophilia	98.82
	Haliscomenobacter sp.	97.50

modified the community profile of the microorganisms during MBR operation.

Filterability of Microbial Flocs

As the microorganisms in HDO and LDO were different, they might have different filtration characteristics. The filterability of microbial flocs existing in each bulk phases was examined. Specific cake resistances of mixed liquors from LDO MBR and HDO MBR were measured to compare the hydraulic properties of microbial flocs. As seen from Fig. 4, the specific cake resistance for LDO MBR was about two orders of magnitude greater than that of HDO, which matches with the filtration data in Fig. 2.

Figure 4 also indicates that the microbial flocs in LDO MBR are more compressible than those in HDO MBR. The compressibility of microbial flocs was calculated using the following equation:

$$\alpha_c = \alpha_0(\Delta P)^n \tag{2}$$

where α_0; the specific cake resistance under one atmospheric pressure, ΔP; the transmembrane pressure, n; the compressibility index. Using the data in Fig. 4, the compressibility indexes for biofilms in LDO and HDO MBRs were calculated to be 0.83 and 0.58, respectively.

The difference in compressibilities of microbial flocs in HDO and LDO MBR may be attributed to their structural difference. Fractal dimension can be used to characterize highly porous amorphous structure of biological flocs in water. Using the laser light scattering technique, the fractal dimensions of the microbial flocs for HDO and LDO MBR were measured to be 2.36 and

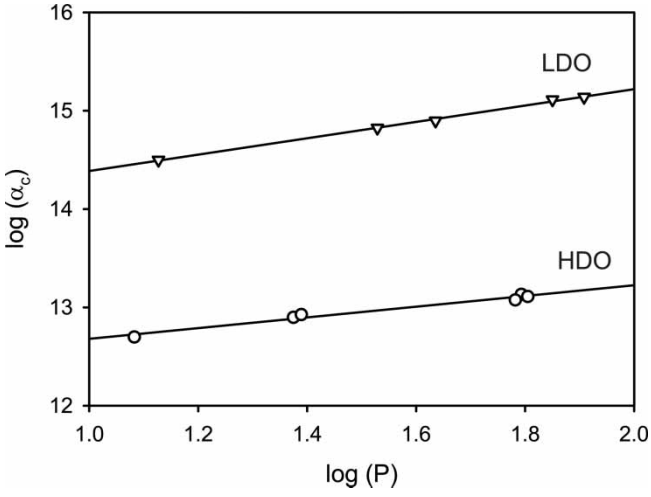

Figure 4. Specific cake resistance in HDO and LDO MBRs.

2.03, respectively. Since the flocs with lower fractal dimension may easily collapse under pressure filtration (27), these structural differences might be one reason for higher compressibility of microbial flocs in LDO MBR.

Biofilm Structure

The hydraulic properties of mixed liquor may be used to predict the permeability through the biofilm. However, characterization of biofilm rather than mixed liquor was necessary to further understand membrane fouling phenomena occurring in the biofilm because the physicochemical and microbial characteristics of biofilm may be different from those of mixed liquor.

Figure 5 shows the cross-sectional images of biofilms on membrane in each reactor. The images were taken after the MBR operation was terminated at 30 kPa. The thickness of HDO-biofilm (214 μm) was greater than that of LDO-biofilm (74 μm) although these two biofilms had similar cake resistances as shown in Table 4. It matches well with the specific cake (biofilm) resistance of microbial flocs in mixed liquor shown in Fig. 4.

To further investigate the structure of the biofilm, images of biofilm obtained using CLSM were analyzed using an image structure analysis program (ISA-2). Examples of CLSM images for the biofilms were shown in Fig. 6. The green, red, and blue parts indicate cells, polysaccharides, and proteins, respectively.

The average porosity for microbial cells was calculated from the image analysis of CLSM pictures. The average porosity for HDO-biofilm was

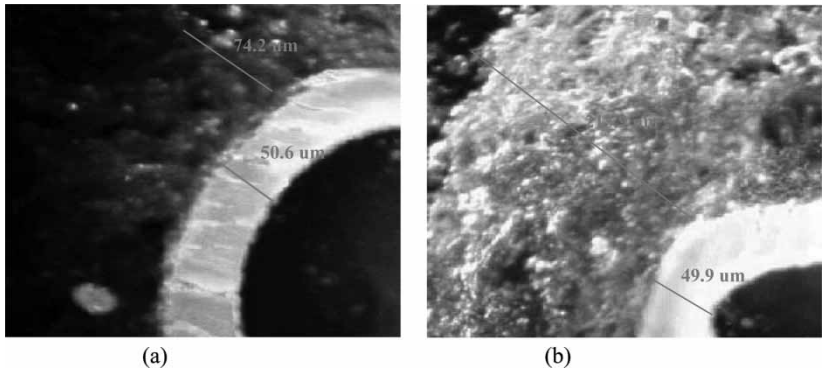

Figure 5. Cross-sectional images of biofilm on membrane: (a) HDO and (b) LDO.

0.87 ± 0.08 whereas that for LDO-biofilm was 0.78 ± 0.09. Similar results were reported by Yun (28). Because specific cake resistance (α) is inversely proportional to the porosity, higher porosity of HDO-biofilm may lead to lower α value, which resulted in better filterability of HDO-biofilm than that of LDO-film. Lower thickness (Fig. 5) and lower porosity for LDO-biofilm may be attributed to the higher compressibility for microbial flocs in LDO MBR. The microbial flocs in LDO MBR were more compressible and thus may form more compact biofilm under high pressure.

Using the image analysis technique, it is also possible to obtain the profile of cell porosity as a function of biofilm depth as well as the average cell porosity. Figure 7a shows the depth profile for cell porosity in each biofilm. The results were expressed as a function of relative thickness,

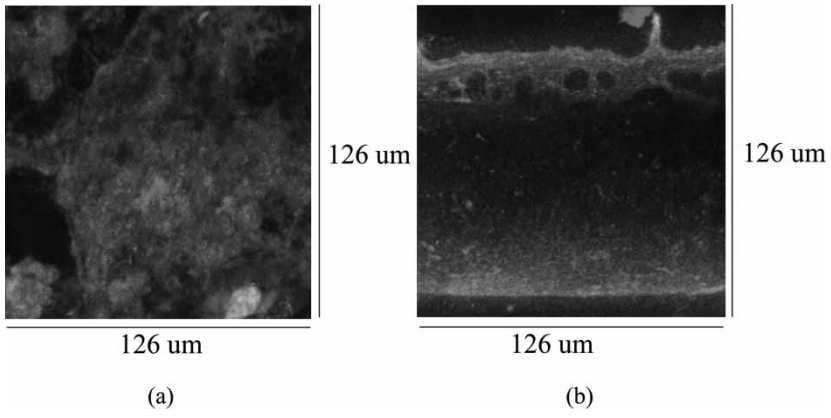

Figure 6. Triple staining on biofilm (red: polysaccharide, blue: protein, green: cell) ($\times 600$): (a) HDO and (b) LDO.

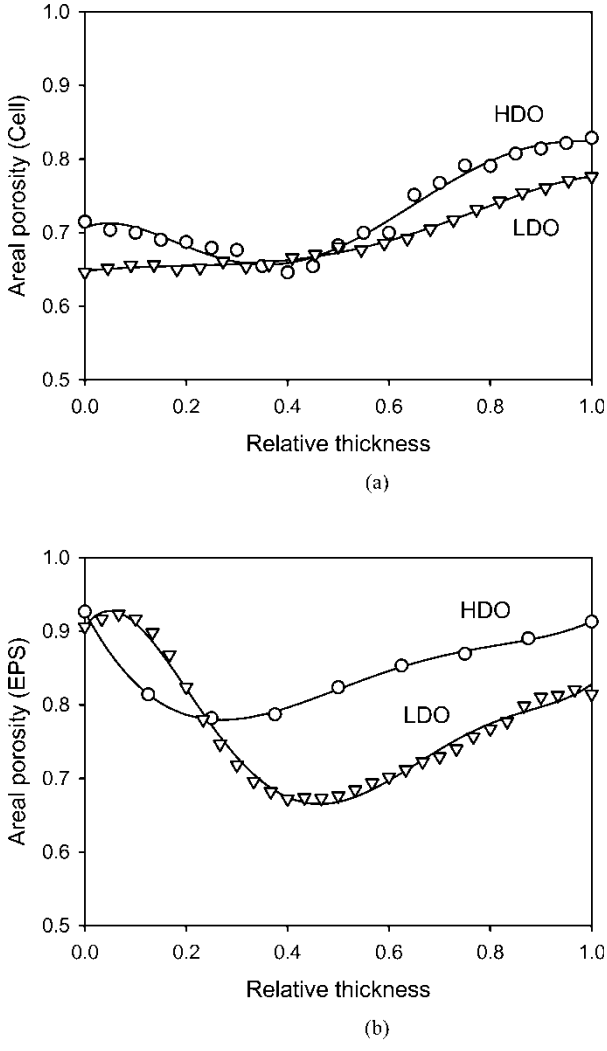

Figure 7. Profiles for areal porosity in HDO- and LDO-biofilm: (a) Cell (b) EPS.

which is defined as the actual depth from the membrane surface divided by total thickness because two biofilms had different thicknesses at the same TMP of 3 kPa (Fig. 5). The profiles for cell porosity also indicate that the cell porosity of LDO-biofilm was smaller than that of HDO-biofilm. The cell porosity increases with relative thickness in LDO-biofilm whereas the cell porosity was the smallest in the middle in HDO-biofilm. This shows that the porosity profile is not uniform and the biofilm structure is heterogeneous.

Distribution of EPS in Biofilm

Same image analysis technique was applied to calculate the depth profiles for EPS porosity in addition to cell porosity. As shown in Fig. 7b, the EPS porosity decreases and then increases after a certain point as the relative thickness increases in both biofilms. The EPS porosity in LDO-biofilm was substantially lower that in HDO-biofilm. This indicates that the distribution of EPS is also heterogeneous like cells.

To examine the EPS distribution inside the biofilm, the coverage ratio of EPS to cell was calculated from the profiles of cell and EPS porosities. In Fig. 8, the results were expressed as a function of relative thickness. The coverage ratio (β), which is defined as the ratio of EPS coverage to cell coverage, was estimated to demonstrate the relative concentration of EPS per unit cell volume in a biofilm using the following equation:

$$\beta = \frac{1 - \varepsilon_{EPS}}{1 - \varepsilon_{cell}} \tag{3}$$

where ε_{EPS}; areal porosity of EPS, ε_{cell}; areal porosity of microbial cells. Here, the coverage ratio of EPS to cell indicates the relative concentration of EPS per unit cell volume in a biofilm.

As shown in Fig. 8, the coverage ratio of EPS for LDO-biofilm was greater than that for HDO-biofilm except the vicinity of membrane surface, indicating that LDO-biofilm had greater amount of EPS per cell. The coverage ratio for HDO-biofilm was almost constant with the relative thickness beyond the relative thickness of 0.2, whereas the coverage ratio for LDO-biofilm changed significantly with the relative thickness. Especially, upper part (e.g., above the relative thickness of 0.4) of the LDO-biofilm has

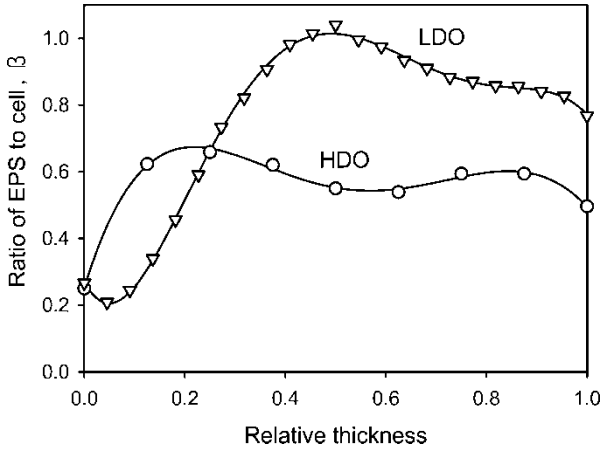

Figure 8. Profiles for the ratio of EPS to cell in HDO- and LDO-biofilm.

larger amount of EPS. Although further study will be necessary, it is likely that the different special distributions of EPS inside biofilm between HDO- and LDO-biofilms may be closely related to the different permeability of the biofilms.

Quantitative and Qualitative Analysis of EPS in Mixed Liquor and Biofilm

The analysis of biofilm indicates that the amount and distribution of EPS in two biofilms were different. Hence, the quantitative analysis of EPS in mixed liquor and biofilm were made to verify the image analysis data shown in Fig. 7b and Fig. 8. The EPS concentrations were expressed as specific weight with the unit of mg EPS per g MLVSS. As shown in Table 6, the total amount of EPS in the bulk phase was 172.2 mg/g MLVSS in HDO MBR and 235.6 mg/g MLVSS in LDO-MBR. Thus, the ratio of total EPS between LDO and HDO MBR was 1.36. The EPS in the biofilm layer on the membrane surface at TMP of 30 kPa were extracted and measured. Total amount of EPS in HDO-biofilm was 125.7 mg/g MLVSS, whereas that in LDO-biofilm was 389.8 mg/g MLVSS. As expected, total amount of EPS in LDO-biofilm was greater than that in HDO-biofilm, which was coincident with the image analysis result. In this case, the ratio of total EPS between LDO and HDO biofilm was 3.11, which is more than two times greater than the ratio (1.36) for the mixed liquor. This result also suggests that the ratio of EPS between mixed liquor and biofilm were quite different for both HDO and LDO MBR. Further studies will be required to elucidate why LDO-biofilm had higher amount of EPS than microbial flocs in bulk phase, but HDO-biofilm did not.

The ratios of proteins to polysaccharides of EPS in HDO- and LDO-biofilm were 2.04 and 0.40, respectively, indicating that the ratio of proteins to polysaccharides in HDO-biofilm are higher than that in LDO-biofilm. These results are in accordance with the previous study by Ma (14).

Table 6. EPS concentration in bulk phase and biofilm

	Polysaccharide		Protein		Total EPS
	Soluble	Bound	Soluble	Bound	(mg/g-MLVSS)
HDO (mixed liquor)[a]	1.2	49.4	1.2	120.3	172.2
LDO (mixed liquor)[a]	2.0	82.5	9.6	141.5	235.6
HDO (biofilm)[b]	41.4		84.3		125.7
LDO (biofilm)[b]	279.4		110.4		389.8

[a]Number of samples for the analysis of EPS in bulk phase, n = 4.
[b]Number of samples for the analysis of EPS in biofilm, n = 3.

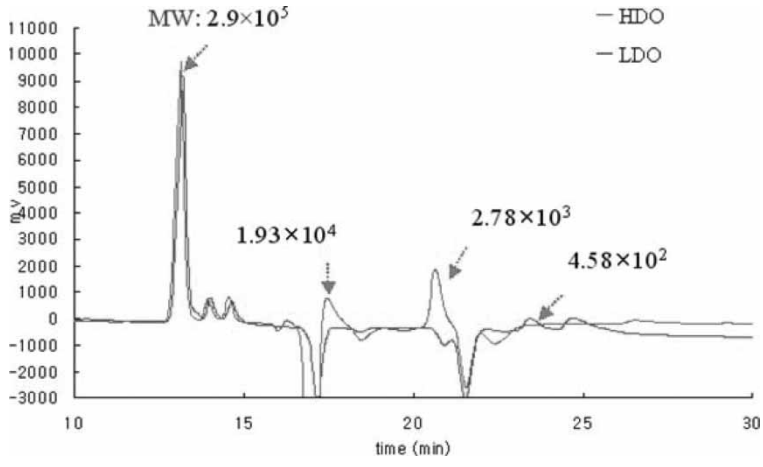

Figure 9. GFC spectrum of soluble EPS components in HDO and LDO MBRs.

Since microbial community structures for two MBRs were different, it was expected that not only the quantity but also the composition of EPS in HDO and LDO MBR would be different. Thus, the molecular weight distribution of soluble portion of each mixed liquor was analyzed using GFC. Figure 9 compares the GFC results for soluble EPS in both MBRs. The peaks for HDO were different from those for LDO after 18 and 21 min, respectively. Two kinds of EPS molecules having 2.78×10^3 Dalton and 1.93×10^4 Dalton were additionally identified in LDO MBR, which seem to be unique EPS compounds in LDO MBR. This suggests that the composition as well as quantity of EPS were different between HDO and LDO MBR.

CONCLUSIONS

In this study, the structural characteristics and composition of biofilms and EPS were investigated for better understanding of membrane fouling in MBR systems under different DO conditions. The following conclusions were drawn:

1. Difference in DO conditions changed the microbial community structures. This led to lower membrane permeability in LDO MBR than HDO MBR. Same microorganisms were found in mixed liquor and biofilm in both MBRs.
2. Microbial flocs in LDO MBR had higher specific cake resistance and compressibility than those in HDO MBR.
3. The porosities for cells and EPS in LDO-biofilm were lower than in HDO-biofilm. Also their distributions inside the biofilm were different from each other.

4. The compositions as well as quantities of EPS were different between HDO and LDO MBR.

ACKNOWLEDGEMENTS

The authors thank the Korean Ministry of Science & Technology for their financial support under Grant M6-0403-00-0098. The authors also thank the National Instrumentation Center for Environment Management (NICEM) for the use of confocal laser scanning microscope system.

REFERENCES

1. Fane, A.G. (1996) Membranes for water production and wastewater reuse. *Desalination*, 106: 1–9.
2. Fang, H.H.P. and Shi, X. (2005) Pore fouling of microfiltration membrane by activated sludge. *J. Membr. Sci.*, in press.
3. Mulder, M. (1996) *Basic Principles of Membrane Technology*; Kluwer Academic Publishers.
4. Clech, P.L., Jefferson, B., and Jude, S.J. (2003) Impact of aeration, solids concentration and membrane characteristics on the hydraulic performance of a membrane bioreactor. *J. Membr. Sci.*, 218: 117–129.
5. Magara, Y. and Itoh, M. (1991) The effect of operational factors on solid/liquid separation by ultramembrane filtration in a biological denitrification system for collected human excreta treatment plants. *Water Sci. Technol.*, 23: 1583–1590.
6. Chang, I.S. and Lee, C.H. (1998) Membrane filtration characteristics in membrane-coupled activated sludge system—the effect of physiological states of activated sludge on membrane fouling. *Desalination*, 120: 221–233.
7. Huang, X., Liu, R., and Qian, Y. (2000) Behavior of soluble microbial products in a membrane bioreactor. *Process Biochem.*, 36: 401–406.
8. Lee, W.T., Kang, S.T., and Shin, H.S. (2003) Sludge characteristics and their contribution to microfiltration in submerged membrane bioreactor. *J. Membr. Sci.*, 216: 217–227.
9. Ishiguro, K., Imai, K., and Sawada, S. (1994) Effects of biological treatment conditions on permeate flux of UF membrane in a membrane/activated-sludge wastewater treatment system. *Desalination*, 98: 119–126.
10. Jin, B., Wilen, B.-M., and Lant, P. (2004) Impacts of morphological, physical and chemical properties of sludge flocs on dewaterability of activated sludge. *Chem. Eng. J.*, 98: 115–126.
11. Kang, I.J., Lee, C.H., and Kim, K.J. (2003) Characteristics of microfiltration performance in a membrane-coupled sequencing batch reactor system. *Water Res.*, 37: 1192–1197.
12. Wilen, B.-M. and Peter, B. (1998) The effect of dissolved oxygen concentration on the structure, size and size distribution of activated sludge flocs. *Water Res.*, 33: 391–400.
13. Kang, I.J. and Lee, C.H. (2004) Effect of aerobic period on microfiltration performance in a membrane-coupled sequencing batch reactor. *J. Ind. Eng. Chem.*, 10 (1): 146–151.

14. Ma, B.-C., Lee, Y.-n., Park, J.-S., Lee, C.-H., and Lee, S.-H. (2004) Correlation between dissolved oxygen concentration, microbial community and membrane permeability in membrane bioreactor, *IWA 4th World Water Congress*. 19th–24th September. Marrakech, Morocco.
15. Choo, K.H. and Lee, C.H. (1998) Hydrodynamic behavior of anaerobic biosolids during crossflow filtration in the membrane anaerobic bioreactor. *Water Res.*, 32 (11): 3387–3397.
16. Okabe, S., Satoh, H., and Watanabe, W. (1999) In-situ analysis of nitrifying biofilms as determined by in-situ hybridization and the use of microelectrodes. *Appl. Environ. Microbiol.*, 3182–3191.
17. Neu, T.R. and Lawrence, J.R. (1999) Lectin-binding analysis in biofilm system. *Method Enzymol.*, 310: 145–152.
18. Strathmann, M., Wingender, J., and Flemming, H.-C. (2002) Application of fluorescently labeled lectins for the visualization and biochemical characterization of polysaccharides in biofilms of Pseudomonas Aeruginosa. *J. Microbiol. Methods*, 50: 237–248.
19. Beyenal, H., Donovan, C., Lewandowski, Z., and Harkin, G. (2004) Three-dimensional biofilm structure quantification. *J. Microbiol. Methods*, 59: 395–413.
20. Staudt, C., Horn, H., Hempel, D.C., and Neu, T.R. (2004) Volumetric measurements of bacterial cells and extracellular polymeric substance glycoconjugates in biofilm. *Biotechnol. Bioeng.*, 88: 585–592.
21. APHA, AWWA, WEF. (1998) *Standard Methods for the Examination of Water and Wastewater*, 2nd Ed. Am. Public Health Assoc. Washington D.C.
22. Lee, J., Ahn, W.-Y., and Lee, C.-H. (2001) Comparison of the filtration characteristics between attached and suspended growth microorganisms in submerged membrane bioreactor. *Water Res.*, 35 (10): 2435–2445.
23. Waite, T.D., Schäfer, A.I., Fane, A.G., and Heuer, A. (1999) Colloidal fouling of ultrafiltration membranes: Impact of aggregate structure and size. *J. Colloid Interface Sci.*, 212: 264–274.
24. Park, J.S. and Lee, C.H. (2005) Removal of soluble COD by a biofilm formed on a membrane in a jet loop type membrane bioreactor. *Water Res.*, 39: 4609–4622.
25. Dubois, M., Gilles, K.A., Hamiltin, J.K., Rebers, P.A., and Smith, F. (1956) Colorimetric method for determination of sugars and related substances. *Anal. Chem.*, 28: 350–356.
26. Frolund, B., Palmgren, R., Keiding, K., and Nielsen, P. (1996) Extraction of extracellular polymers from activated sludge using a cation exchange resin. *Water Res.*, 30: 1749–1758.
27. Park, P.K., Lee, S., and Lee, C.H. (2004) Permeability dependence of cake formed by chemical flocs on coagulation conditions in coagulation-membrane processes. *Water Environment—Membrane Technology 2004 (WEMT2004)*. Seoul, Korea; Vol. 3, 903–910.
28. Yun, M.-A., Yeon, K.-M., Park, J.-S., Lee, C.-H., Chun, J., and Lim, D.J. (2005) Characterization of biofilm structure and its effect on membrane permeability in MBR for dye wastewater treatment. *Water Res.*, in press.